Singularities & Dynamical Systems
S.N. Pnevmatikos (editor)

#36

BIFURCATIONS AND CHAOS IN FORCED VAN DER POL SYSTEMS

Ralph Abraham & Carles Simó

University of California, U. S. A.

Universitat de Barcelona, SPAIN

The Van der Pol system, modified through the addition of constant force and bias terms and explored through simulation, reveals an unsuspected bifurcation of codimension two. Forcing the system yields an abundance of chaotic attractors and bifurcations.

1. INTRODUCTION

We began our simulations with the intent to illustrate the bifurcation sequences of codimension one, described in the companion paper [1]. These illustrations reveal the detailed structure of the *red cigar* (Sec. 2, Figs. 1-5) and the *blue sleeve* (Sec. 3, Figs. 6-11). Unable to resist the temptation to explore further, we added sinusoidal forcing to the standard shift, and discovered an abundance of chaotic attractors and bifurcations, very similar to the sequence studied by Rossler [2] (Sec. 4, Figs. 12-17). Finally, combining the two bias parameters without forcing, we mapped the full bifurcation set in the control plane, finding the *blue goblet*, an unsuspected bifurcation of codimension two (Sec. 5, Figs. 18-22). This appears to be identical to one discovered by Takens [3; 5, p. 371] and found in a related context by Fitzhugh [11], Guckenheimer and others [4; 5, p. 70].

2. STANDARD BIAS

The equations under consideration are

$$\dot{x} = y,$$

$$\dot{y} = -x + \epsilon(1 - x^2)y + a,$$

$\epsilon > 0$, $a \in R$. The system has the trivial symmetry $(x,y,a) \leftrightarrow (-x,-y,-a)$. It has only one critical point, $P = (a,0)$. Figure 1 gives the locus of $\dot{y} = 0$ for $a = 0, 0.9, 1, 1.1, 2$ and $\epsilon = 1$. Note that every line $y =$ constant has, at most, two cuts with the graphs shown in Figure 1.

Figure 2 displays the linear character of P as a function of (ϵ,a). It turns out that this system has exactly one periodic orbit and that it is the only attractor of the system for $a \in (-1,1)$ for any $\epsilon > 0$. For $a \in (-\infty,-1] \cup [1,\infty)$ the only attractor is P.

Figure 3 shows some of these orbits for $\epsilon = 1$ and values of a equal to -.99, -.96, -.84, -.5, 0, .5, .84, .96, .99. For the same value of ϵ in Figure 4 we present the section of the current attractor as a function of a. The family of periodic orbits (PO) can be seen as a *cigar*. In Figure 5 the plot of the period T of the PO against a is shown. The amplitude $(x_{sup} - x_{inf})$ of the PO has a quadratic behavior when $a \to \pm 1$.

Figures 3 bis, 4 bis and 5 bis are obtained when ϵ is set equal to 4. In Figure 3 bis the displayed POs have values of a equal to -0.999, -0.9926, -0.991776, -0.99177072, -0.99177071, -0.9917707, -0.99, -0.5 and 0, respectively. Symmetrical figures are obtained for positive values. The selected values are chosen to display the well known *canard effect* due to the presence of a slow manifold [6]. This effect is hard to see in Figures 4 bis and 5 bis. However it can be checked in Table 1, which offers some numerical data to reproduce Figures 3 bis to 5 bis.

3. VELOCITY BIAS

We merely move the bias to the first equation. The behavior of the system changes in a dramatic way. The equations are

$$\dot{x} = y - c,$$

$$\dot{y} = -x + \epsilon(1 - x^2)y,$$

$\epsilon > 0$, $c \in \mathbf{R}$, with the trivial symmetry $(x,y,c) \leftrightarrow (-x,-y,-c)$. We always suppose $c \neq 0$. Two critical points appear, $P_\pm = (x_\pm,c)$, where

$$x_\pm = -\frac{1}{2\epsilon c} \pm \left(\frac{1}{4\epsilon^2 c^2} + 1\right)^{1/2}.$$

Note that, letting c go to zero, one of the points goes to the origin and the other escapes to infinity.

The linear behavior of P_+ is shown in Figure 6 as a function of (ϵ,c). It is always a repellor for $\epsilon > 0$. P_- is always a dissipative saddle (i.e., a saddle such that the divergence is negative at it). Figure 7 displays the invariant stable and unstable manifolds of P_- for the following couples of (ϵ,c):

(1,0.5), (1,0.6), (4,0.1), (4,0.2), (0.25,1.8) and (0.25,2.2).

According to our numerical results it seems that for every $\epsilon > 0$ there is exactly one positive c (and, of course, this happens also for -c) such that there exists a homoclinic orbit to P_-. Let $c^*(\epsilon)$ be this value. In Figure 8 we present the curve $c^*(\epsilon)$. Table 2 offers some of the related numerical data.

Now we fix $\epsilon = 1$. The attracting POs present for c = 0 can be continued in the range $(-c^*(1), c^*(1))$ and it is (according to numerical simulation) the only attractor in this range. The family of POs terminates at each end in the homoclinic orbit (the so-called blue sky catastrophe) and, accordingly, the period T goes to $+\infty$. We shall call this family a . For $c \in (-\infty, -c^*(\epsilon)) \cup (c^*(\epsilon), \infty)$ there is no attractor. Figure 9 shows the PO for c = -.569, -.4, -.2, .4, .569. Figures 10 and 11 are similar to Figures 4 and 5. For $\epsilon = 4$ the results are given at Figures 9 bis (for c = -.159, -.13, -.07, .07, .13, .159), 10 bis and 11 bis. Finally Table 3 offers the related numerical data.

4. STANDARD BIAS WITH FORCING

Here we consider the following equations:

$$\dot{x} = y,$$

$$\dot{y} = -x + \epsilon(1 - x^2)y + a + b\cos\omega t$$

Next we describe the results of a rough exploration by simulation. For $(\epsilon, a, b, \omega) = (4,1,2,3)$, starting at (0,0) for t = 0 the orbit becomes attracted by a stable PO. Throughout the exploration we keep $(\epsilon, a, \omega) = (4,1,3)$. Slowly varying b and starting each simulation at the previous attractor one gets a sequence of period-doubling bifurcations. Figure 12 shows, for b = 2, 2.5, 2.84 and 2.87, orbits which we call 1-PO, 2-PO, 4-PO and 8-PO because they are seen as 1, 2, 4, 8 periodic points under the time $-\frac{2\pi}{\omega}$ map (that we design as F).

A slight further increment of b to 2.88 gives what seems to be a 32 piece strange attractor (32-SA). Figure 13 displays the points obtained using F and magnifications. Then we have an inverse cascade of fusions of attractors (see [2, 7, 8, 9]). Figures 14, 15 and 16 show the 4-SA (for b = 2.885), the 2-SA (for b = 2.89) and the orbit for b = 2.89, respectively.

A further increase to 2.9 shows that the SA is destroyed (of course, by heteroclinic tangency, see [7]) and we observe an attracting 7-PO. Figure 17 displays this orbit for b = 2.9, 2.8, 2.6. Now we can go backwards in b. This

attracting 7-PO exists till some value near 2.5 for which the orbit disappears through a saddle-node bifurcation. The stable manifold of the corresponding saddle bounds the basin of attraction. It is the transversality of this manifold with the SA, which seems to be the closure of the unstable manifold of a 2-PO of saddle type (the one obtained by continuation of the previously attracting 2-PO), the reason of the destruction of the SA. Then two different attracting POs, or an attracting PO and an SA, can simultaneously coexist. The basins of some of these attractors can be small and difficult to detect if random initial conditions are chosen. Further analysis will be the object of a future paper. Table 4 gives initial conditions (t = 0) for the displayed figures.

5. DOUBLE BIAS

In this section we combine the two previously studied biases. It will be apparent that the symmetry existing before in the termination of the family of attracting POs can be destroyed.

The standing equations are

$$\dot{x} = y - c,$$

$$\dot{y} = -x + \epsilon(1 - x^2)y + a, \quad \epsilon > 0$$

with symmetry $(x,y,a,c) \longleftrightarrow (-x,-y,-a,-c)$. We can suppose $a,c \neq 0$, the other cases being already discussed, and even we can suppose $c > 0$. The critical points are $P_{\pm} = (-\frac{1}{2\epsilon c} \pm (\frac{1}{4\epsilon^2 c^2} + 1 + \frac{a}{\epsilon c})^{1/2}, c)$. They exist if

$$a > -\epsilon c - \frac{1}{4\epsilon c} \qquad (*)$$

(for positive ϵc). P_+ always has index +1 and P_- is always a saddle. The linear character of $P_{\pm}$ is given in Figure 18, P_- expansive means div $X(P_-) > 0$. When equality holds in (*), only one critical point appears. In Figure 18 we also show the curve $\varphi(a,c) = 0$ (for $\epsilon = 1$) for which we get a homoclinic connection. A similar picture for $\epsilon = 4$ is given in Figure 18 bis. Table 5 offers numerical data for the figures. Table 6 presents values of (ϵ,a) producing homoclinic orbits for increasing values of c.

Let us analyze the neighborhood of the point $a = -1$, $\epsilon c = 1/2$ in the parameter space. First set $a = -1$, $\epsilon c = 1/2$ and change variables through $\xi = x + 1$, $\eta = y - \frac{1}{2\epsilon}$. We get $\dot{\xi} = \eta$, $\dot{\eta} = \xi(2\epsilon\eta - \epsilon\eta\xi - \xi/2)$. We note $\dot{\eta} = 0$ if $\xi = 0$ or $\eta = \frac{\xi/2}{\epsilon(2-\xi)}$. Figure 20 describes the vector field. For a fixed $\eta > 0$ the

maximum of $\dot{\eta}$ is obtained for $\xi = \frac{2\epsilon\eta}{1+2\epsilon\eta}$. Then $\dot{\eta} < 2\epsilon\eta$ and the slope in A is less than 2ϵ. A similar result is obtained for $\eta < 0$, $\xi \in (0,2)$, bounding the slope for large enough values of $-\eta$. Therefore, flow entering through the positive η axis escapes through the positive ξ axis, and, after, through the negative η axis. Forward and backward images of the negative ξ axis go to W^u, W^s. Local expressions for $W^{u,s}$ near (0,0) are

$$\eta = \Psi^o_{u,s}(\xi) = a_o(-\xi)^{r_o} + a_1(-\xi)^{r_1} + \ldots,$$

$r_1 > r_o$, $r_o = 3/2$, $a_o = \pm 3^{-1/2}$. For $\xi \to -\infty$ we get

$$W^s: \quad \eta = \Psi^\infty_s(\xi) = b_o(-\xi)^{s_o} + b_1(-\xi)^{s_1} + \ldots,$$

$s_1 < s_o$, $s_o = 3$, $b_o = -\frac{\epsilon}{3}$, and

$$W^u: \quad \eta = \Psi^\infty_u(\xi) = c_o(-\xi)^{t_o} + c_1(-\xi)^{t_1} + \ldots$$

$t_1 < t_o$, obtaining $\Psi^\infty_u(\xi)$ = hyperbola + $\epsilon^{-2}/2\xi^{-4} + \ldots$, where hyperbola means the locus of $\eta = 0$,

$$-\frac{1}{2\epsilon} + \frac{1}{\epsilon}(-\xi)^{-1} - \frac{2}{\epsilon}(-\xi)^{-2} + \frac{4}{\epsilon}(-\xi)^{-3} - \frac{8}{\epsilon}(-\xi)^{-4} + \ldots .$$

A sketch of $W^{u,s}$ is also given in Figure 20.

We next describe the (global) behavior for $(a,\epsilon c)$ near $(-1,1/2)$.

THEOREM: Near $a = -1$, $\epsilon c = 1/2$, the bifurcation diagram given in Figure 21 holds.

Proof: As the only essential modifications to the flow are near the origin, we only need to examine this region. The proof shall also give quantitative information. We set $\epsilon > 0$, $a = -1 - \alpha$, $c = \frac{1+\beta}{2\epsilon}$ with α,β small. The condition $\frac{1}{4\epsilon^2c^2} + 1 + \frac{\alpha}{\epsilon c} \geq 0$ is written as $\beta^2 - 2\alpha(1+\beta) \geq 0$. Hence, curve (1)-(3) is given by $\alpha = \frac{\beta^2}{1+\beta}$. On this curve the field has a double fixed point as at $(\alpha,\beta) = (0,0)$, and the behavior is the same.

From the fact that there are only two fixed points for $\beta^2 - 2\alpha(1+\beta) > 0$, their character already discussed, the only thing to prove is the location of branch (5) for which we get a homoclinic connection. Let $\gamma^2 = \beta^2 - 2\alpha(1+\beta) > 0$, $\gamma > 0$. We introduce the changes

$$\xi = (2\gamma)^{-1}[(1+\beta)x+1+\gamma], \quad \eta = (2\gamma^{3/2})^{-1}[y-(1+\beta)/2\epsilon], \quad ' = \frac{d}{d\tau} = \gamma^{-1/2}\frac{d}{dt}$$

giving

$$\xi' = (1+\beta)\eta$$

$$\eta' = \frac{1}{1+\beta}(\xi-\xi^2) + 4\epsilon\frac{\beta-\gamma}{\gamma^{1/2}}\frac{1+\frac{\beta+\gamma}{2}}{(1+\beta)^2}\eta + 8\epsilon\gamma^{1/2}\frac{1+\gamma}{(1+\beta)^2}\xi\eta - \frac{8\epsilon\gamma^{3/2}}{(1+\beta)^2}\xi^2\eta$$

Let us introduce $k = (\beta-\gamma)/\gamma$. When $\alpha,\beta \to 0$ (and, hence, $\gamma \to 0$) the dominant term and the main perturbations are

$$\xi' = \eta, \quad \eta' = \xi - \xi^2 + \gamma^{1/2}(4\epsilon k\eta + 8\epsilon\xi\eta).$$

For $\gamma = 0$ this is a hamiltonian system, for $H = \frac{1}{2}\eta^2 - \frac{1}{2}\xi^2 + \frac{1}{3}\xi^3$, with a separatrix given by

$$\xi = \frac{3}{2\cosh^2(\tau/2)}, \quad \eta = -\frac{3\sinh(\tau/2)}{2\cosh^3(\tau/2)}.$$

The Melnikov function [5, Ch. 4; 10] is given by

$$4\epsilon\int_R \begin{vmatrix} \eta & 0 \\ \xi - \xi^2 & k\eta + 2\xi\eta \end{vmatrix}(\tau)d\tau = 4\epsilon\left[k\int_R \eta^2 + 2\int_R \xi\eta^2\right]$$

linear in k. The value of k in order to get connection is $k = \frac{-2\int_R \xi\eta^2}{\int_R \eta^2} =$

$-3\frac{\int_R \sinh^2\cosh^{-8}}{\int_R \sinh^2\cosh^{-6}} = -\frac{12}{7}$. Hence $\beta = -\frac{5}{7}\gamma$, or $\alpha = -\frac{12}{25}\beta^2 + \ldots$ (for $\beta < 0$).

This gives (5). Similar checks give the results concerning periodic orbits. □

This result agrees with numerical simulations (see Table 5). Now we look at the behavior of the homoclinic connections for $c \to \infty$. Using the same method of scaling variables and time, displaying a hamiltonian plus perturbations, after some computations to higher order than before, we get $a = 5/7$. This is the asymptote to the curve $\rho(a,c) = 0$ of homoclinic connections for $c \to \infty$ for any ϵ. This agrees with Figures 18 and 18 bis, and with Table 6. The curve $\rho(a,c) = 0$ never reaches the line $a = 1$, and it seems that for $\epsilon \leq 1$, c increases monotonically when $\alpha \to 5/7$, while for $\epsilon > 1$, a reaches a maximum on $\rho(a,c) = 0$ and then, when decreasing to 5/7, c goes monotonically to ∞.

We return to Figure 18. Single arrows mean Hopf bifurcation and double arrows mean creation of a PO by inverse blue sky catastrophe. The conjecture, supported by the previous analytic discussion and several numerical experiments, is that in $S_1 \cup S_2$ there is a punctual attractor; in Q (unbounded region) the attractor is just one PO, and, in $\mathbb{R}^2-(Q \cup S_1 \cup S_2)$ there is no attractor. A path like c_1, c_2, c_3, c_4 in the parameter space (for any $\epsilon > 0$) produces families of POs, as shown in Figure 19: red cigar, blue sleeve, Hopf-connection (direct goblet) and connection-Hopf (inverse goblet), respectively.

6. ACKNOWLEDGEMENTS

The authors express their gratitude to Dr. Gerard Gomez for his valuable cooperation in the program they used for most of the numerical simulations, to Dr. Bruce Stewart and Prof. John Guckenheimer for pointers to the literature on bifurcations of codimension two, and to Christopher Shaw for Fig. 22. The work of the second author has been partially supported by CIRIT, Univ. de Barcelona and the Univ. Autonoma de Barcelona.

7. BIBLIOGRAPHY

[1] Abraham, R. H., In pursuit of Birkhoff's chaotic attractor, this volume.

[2] Rössler, O., An equation for continuous chaos, Phys. Lett. 57A (1976) 397-398.

[3] Takens, F., Forced oscillations and bifurcations, Comm. Math. Inst., Rijkuniversitat Utrecht 3 (1974) 1-59.

[4] Guckenheimer, J., Dynamics of the Van der Pol equation, IEEE Trans. CAS-27 (1980) 983-989.

[5] Guckenheimer, J. and Holmes, P., Nonlinear Oscillations, Dynamical Systems and Bifurcations of Vector Fields (Springer, New York, 1983).

[6] Diener, M., Canards, ou comment bifurquent les systemes differentials lents-rapides, preprint, CERDRO, BP1510 Saint-Charles, Oran.

[7] Simo, C., On the Henon-Pomeau attractor, J. Stat. Phys. 21 (1979) 456-493.

[8] Simo, C. and Garrido, L., Some ideas about strange attractors, in Dynamical Systems and Chaos, L.N. in Phys. 179 (Springer, New York, 1983) 1-23.

[9] Lorenz, E. N., Noisy periodicity and reverse bifurcation, Ann. New York Acad. Sci. 357 (1980) 282-293.

[10] Marsden, J. E., Chaotic orbits by Melnikov's method: a survey of applications, Proc. 22nd IEEE Conf. Decision & Control (Dec. 1983).

[11] Fitzhugh, R., Thresholds and plateaus in the Hodgkin-Huxley nerve equations, J. Gen. Physiol. 43 (1960) 867-896.

a.	x_{inf}	x_{sup}	Period
0	-2.008620	2.008620	6.6633
.1	-1.946181	2.063823	6.6788
.2	-1.874901	2.112698	6.7258
.3	-1.792173	2.155544	6.8051
.4	-1.693699	2.191935	6.9183
.5	-1.571987	2.220220	7.0660
.6	-1.412658	2.235991	7.2454
.7	-1.184127	2.236798	7.4352
.8	- .807333	2.150291	7.5269
.84	- .581432	2.074460	7.4573
.88	- .303718	1.953738	7.2716
.92	- .011883	1.781628	6.9755
.96	- .360095	1.549512	6.6284
.97	- .458713	1.475628	6.5406
.98	- .568854	1.388712	6.4536
.99	- .703418	1.275994	6.3677

Table 1a: $\epsilon = 1$

a	x_{inf}	x_{sup}	Period
0	-2.022963	2.022963	10.2035
.2	-1.999139	2.044498	10.3458
.4	-1.972056	2.064318	10.8040
.6	-1.939767	2.082796	11.6967
.8	-1.896882	2.100197	13.3698
.88	-1.872418	2.106901	14.4959
.96	-1.831121	2.113474	16.3747
.99	-1.764276	2.115906	18.2484
.9917	-1.684231	2.116033	19.1733
.99177	-1.514461	2.115715	20.0614
.9917706	-1.405560	2.114634	20.3409
.9917707	-1.176177	2.105610	20.5273
.99177071	- .616834	2.010342	19.1280
.99177072	- .162242	1.841492	16.1990
.99177073	- .090650	1.807267	15.6060
.991771	.120522	1.693909	13.6742
.9918	.406494	1.509359	10.7124
.9926	.625961	1.341057	8.3845
.999	.907310	1.090591	6.4244
.9996	.942492	1.056693	6.3379
.9998	.959613	1.039984	6.3103

Table 1b: $\epsilon = 4$

ϵ	$c^*(\epsilon)$
0.1	4.921542
0.2	2.491228
0.3	1.689162
0.4	1.290966
0.5	1.052638
0.7	.779078
1	.569529
2	.307091
3	.210359
4	.159864
5	.128919
7	.092957
10	.065551

Table 2

c	x_{inf}	x_{sup}	Period
.1	−2.024675	1.990147	6.7123
.2	−2.038161	1.969425	6.8719
.3	−2.048942	1.946643	7.1906
.4	−2.056895	1.921988	7.8129
.5	−2.061893	1.895579	9.3739
.55	−2.063237	1.881707	12.1738
.565	−2.063485	1.877454	15.8887
.569	−2.063539	1.876312	21.7364
.5694	−2.063544	1.876198	25.6603
.5695	−2.063546	1.876170	29.8378

Table 3a: $\epsilon = 1$

c	x_{inf}	x_{sup}	Period
.04	−2.027075	2.018759	10.4569
.08	−2.031100	2.014461	11.3751
.12	−2.035040	2.010065	13.8633
.14	−2.036979	2.007830	17.2059
.15	−2.037941	2.006703	21.2342
.155	−2.038420	2.006137	25.8253
.157	−2.038611	2.005910	29.5204
.159	−2.038802	2.005683	38.4049
.1596	−2.038859	2.005615	47.5895
.1598	−2.038878	2.005592	58.7766

Table 3b: $\epsilon = 4$

b	x	4	Fig
2	.996	-.626	12a
2.5	1.003	-.651	12b
2.84	1.013	-.587	12c
2.87	1.013	-.573	12d
2.88	1.015359	-.579361	13
2.885	1.012503	-.564710	14
2.89	1.017725	-.597039	15,16
2.9	1.101703	-.713349	17a
2.8	1.371443	-.382202	17b
2.6	1.15758	-.59054	17c

Table 4

a	c
-.99999952	.4995
-.99999808	.499
-.99999299	.498
-.9999	.49283590
-.999	.47767821
-.99	.43218198
-.98	.40632647
-.95	.36238802
-.9	.33739337
-.8	.34057534
-.5	.40279066
-.3	.45834335
-.1	.52738296
.1	.61948395
.3	.76258556
.45	.96849067
.5	1.09172511
.55	1.28684964
.6	1.65722509
.65	2.64787700
.7	11.0412399
.71	36.476921
.71272558	100
.714	545.626
.71412984	1000

Table 5a: $\epsilon = 1$

a	c
-.999999	.12481588
-.99999	.12439064
-.9999	.12273488
-.999	.10993464
-.995	.08006557
-.99	.08042535
-.9	.08695508
-.7	.10185668
-.5	.11737645
-.3	.13364175
-.1	.15083604
.1	.16924222
.3	.18934203
.5	.21209498
.7	.24005527
.9	.28910545
.95	.34497425
.9541	.38550468
.95414067	.3893
.9541	.39913685
.95	.47743240
.9	1.01942836
.74291038	10
.71722746	100
.71458062	1000

Table 5b: $\epsilon = 4$

ϵ	a
10	.971481
20	.986726
40	.993566
100	.997471

Table 6a: c = 1

ϵ	a
10	.792950
20	.855072
40	.923795
100	.973105

Table 6b: c = 10

ϵ	a
.1	.689450
.2	.702112
.4	.708495
2	.714842
10	.722878
20	.731684
40	.748630
100	.794949

Table 6c: c = 100

ϵ	a
.1	.711841
.2	.713078
.4	.713709
2	.714341
10	.715151
20	.716052

Table 6d: c = 1000

ϵ	a
.1	.713675
.2	.713984
.4	.714142
1	.714247
2	.714300
4	.714359
10	.714502

Table 6e: c = 4000

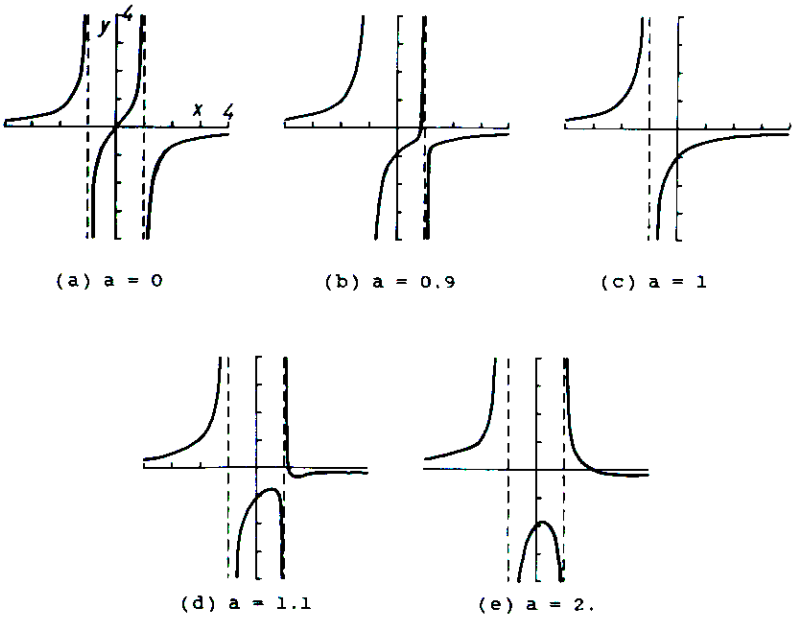

Fig. 1 Characteristic curves with standard bias, $\epsilon = 1$.

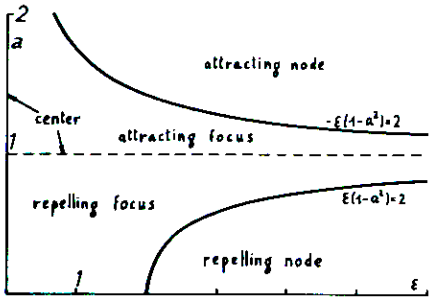

Fig. 2. Qualitative type of the critical point, P, with standard bias.

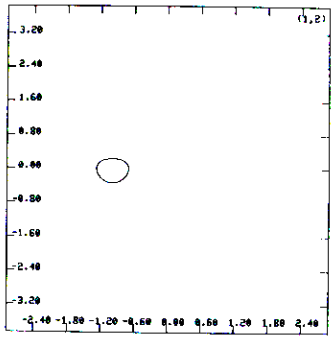

(a) a = −0.99

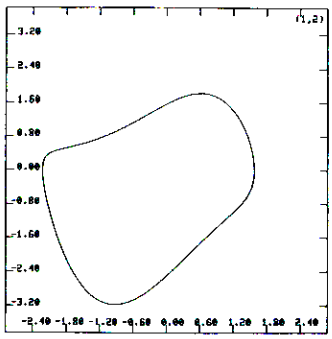

(d) a = −0.50

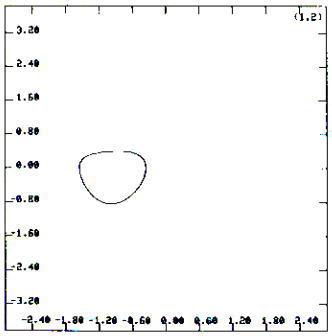

(b) a = −0.96

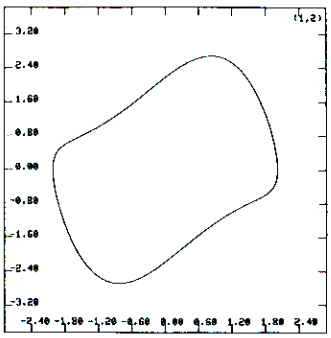

(e) a = 0

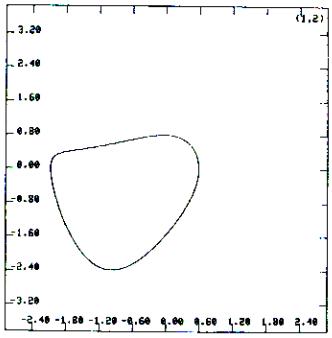

(c) a = −0.84

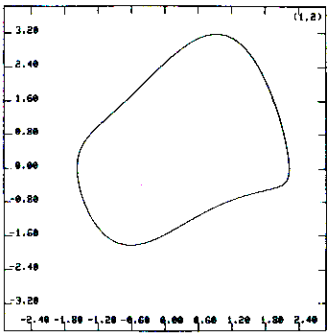

(f) a = 0.50

Fig. 3. Periodic attractors with standard bias, ϵ =1.

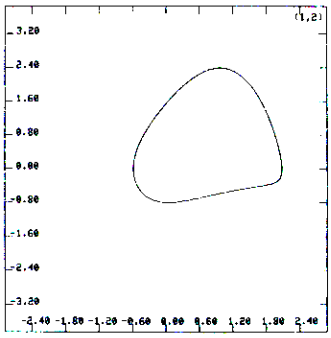

(g) a = 0.84

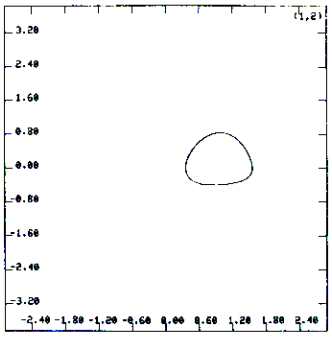

(h) a = 0.96

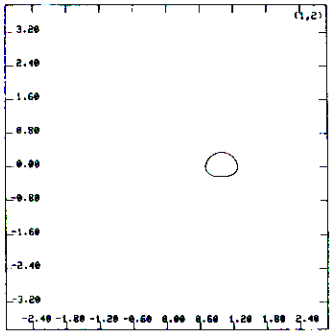

(i) a = 0.99

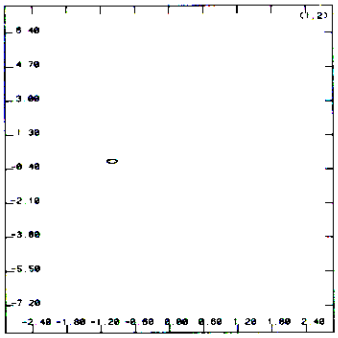

(a) a = -0.0990

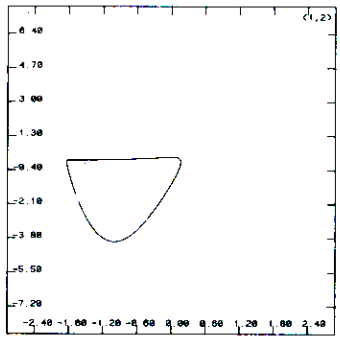

(d) a = -0.99177072

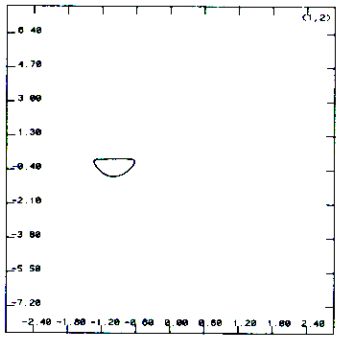

(b) a = -0.9926

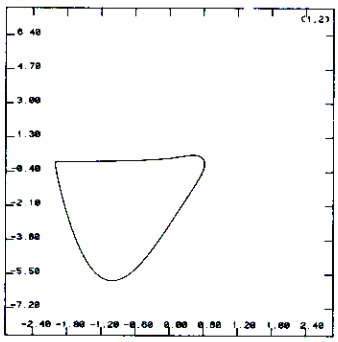

(e) a = -0.99177071

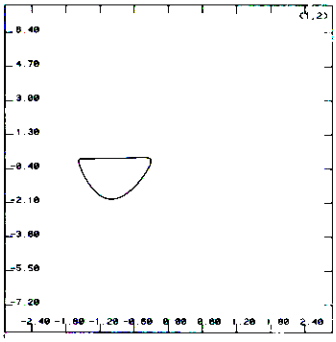

(c) a = -0.991776

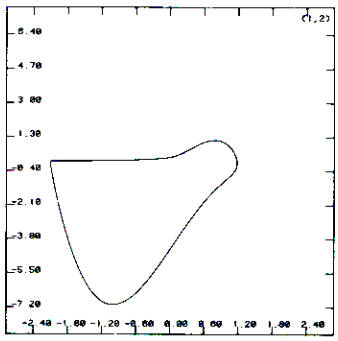

(f) a = -0.99177070

Fig.3 bis. Periodic attractors with standard bias, ϵ =4, showing the canard.

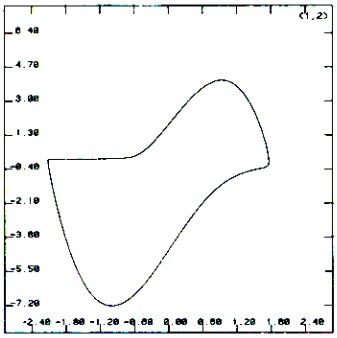

(g) a = −0.990

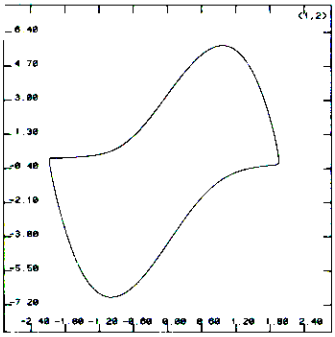

(h) a = −0.5

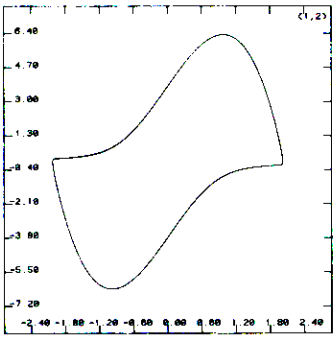

(i) a = 0

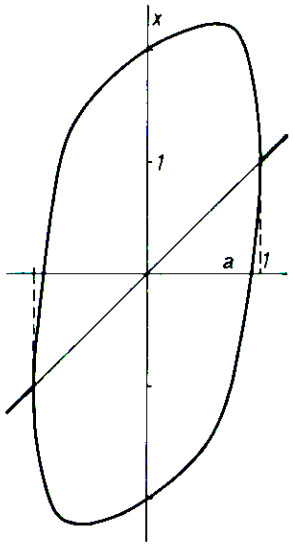

Fig. 4. Cross-section of the red cigar, ϵ =1.

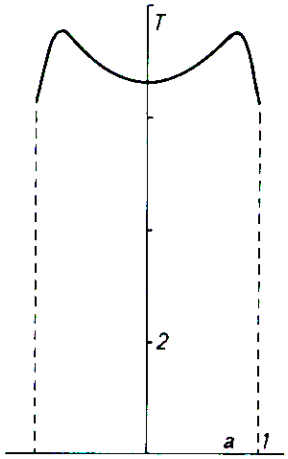

Fig. 5. Periods of the red cigar, ϵ =1.

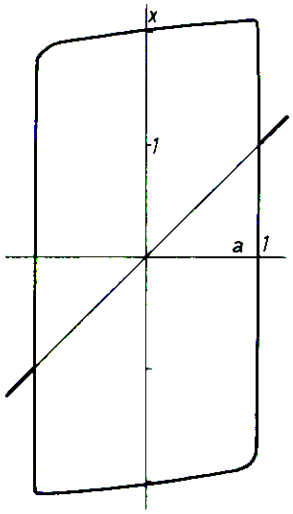

Fig. 4 bis. Cross-section of the red cigar, ϵ =4.

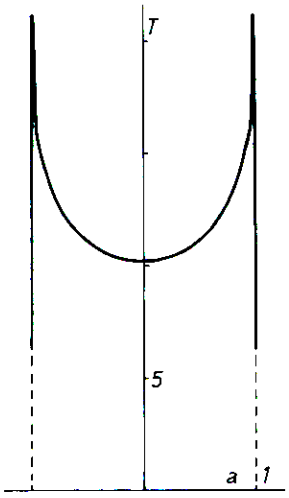

Fig. 5 bis. Periods of the red cigar, ϵ =4.

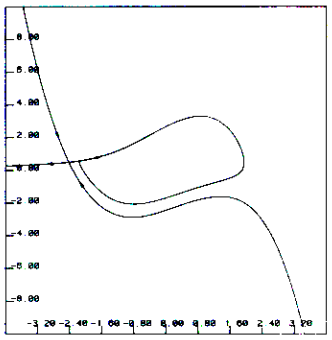

(a) ϵ =1, c = 0.5

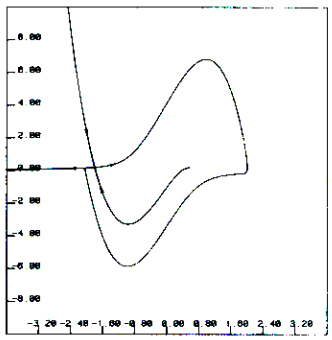

(d) ϵ =4, c = 0.2

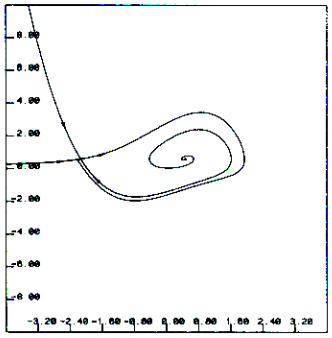

(b) ϵ =1, c = 0.6

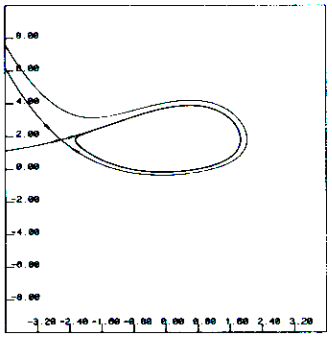

(e) ϵ =0.25, c = 1.8

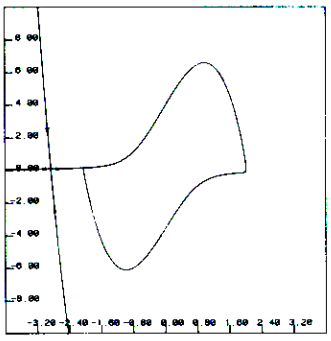

(c) ϵ =4, c = 0.1

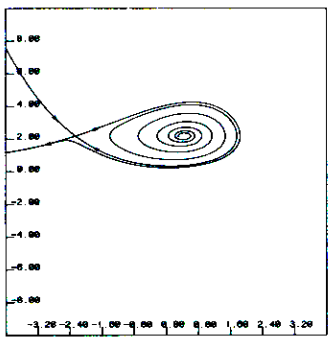

(f) ϵ =0.25, c = 2.2

Fig. 7. Invariant curves of the saddle point, P_{-}, with velocity bias.

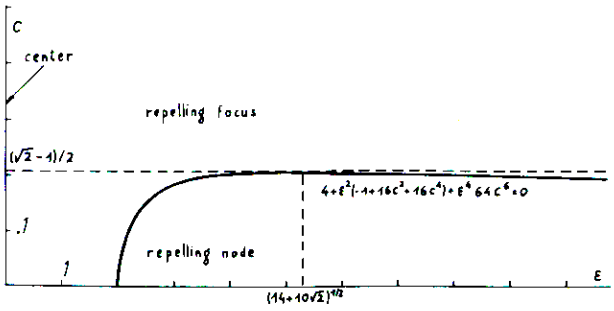

Fig. 6. Qualitative type of the critical point, P_+, with velocity bias.

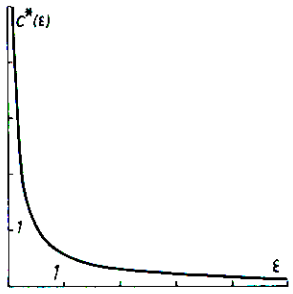

Fig. 8. Velocity bias for the homoclinic saddle connection of P_-.

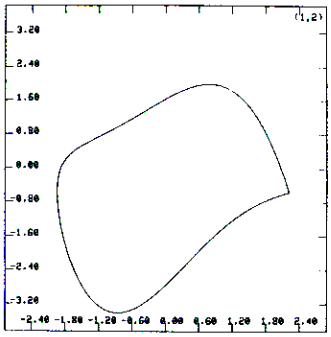

(a) c = −0.569

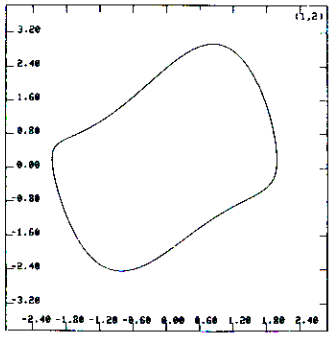

(d) c = 0.2

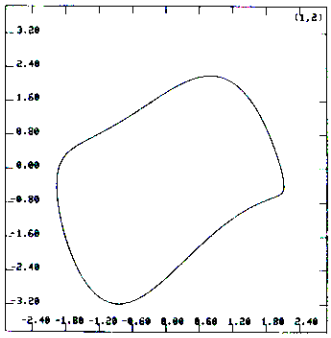

(b) c = −0.4

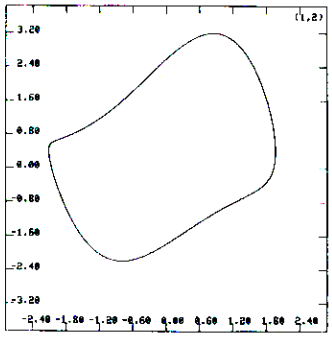

(e) c = 0.4

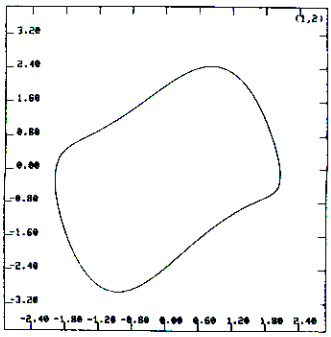

(c) c = −0.2

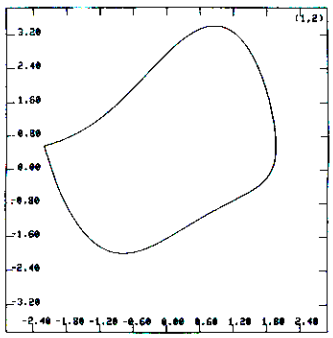

(f) c = 0.569

Fig. 9. Periodic attractors of the blue sleeve, with $\epsilon = 1$ and velocity bias, c.

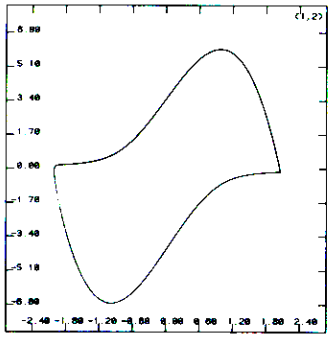

(a) c = −0.159

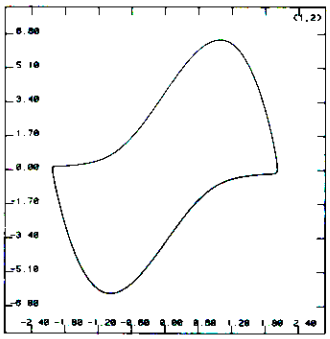

(d) c = 0.07

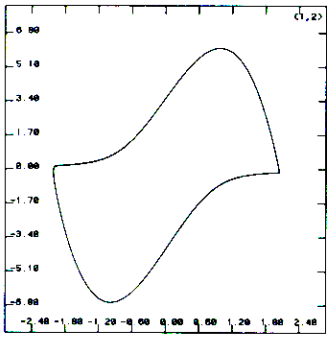

(b) c = −0.13

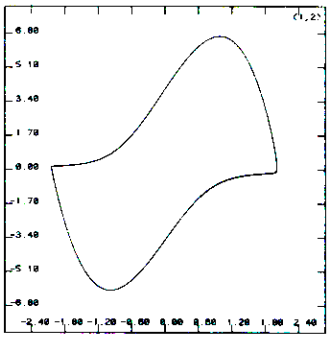

(e) c = 0.13

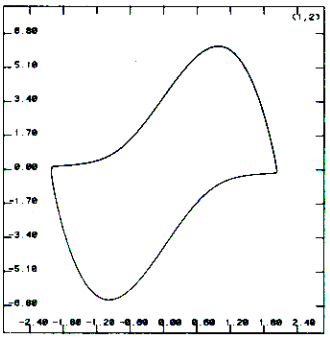

(c) c = −0.07

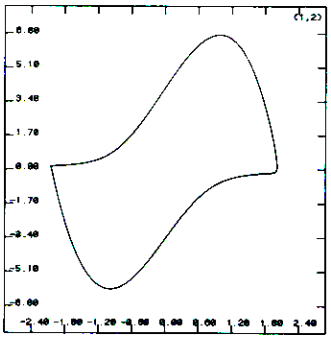

(f) c = 0.159

Fig. 9 bis. Periodic attractors of the blue sleeve, with ϵ =4 and velocity bias, c.

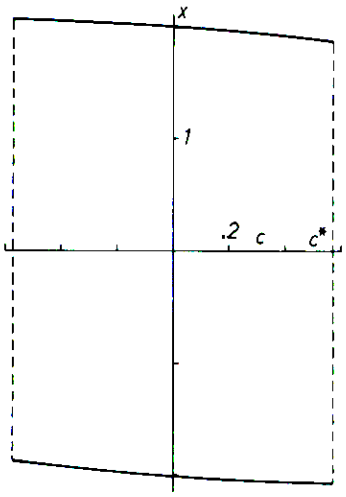

Fig. 10. Cross-section of the blue sleeve, $\epsilon = 1$.

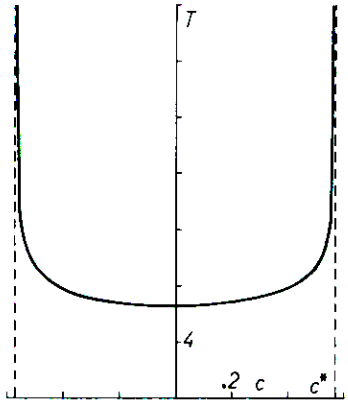

Fig. 11. Periods of the blue sleeve, $\epsilon = 1$.

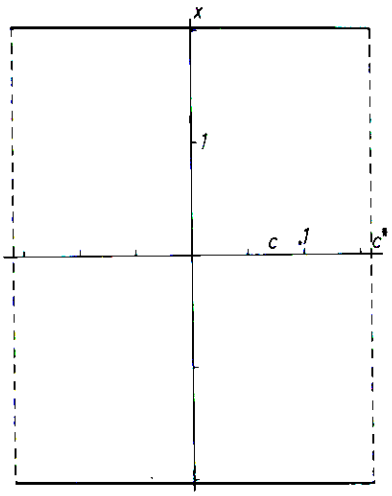

Fig. 10 bis. Cross-section of the blue sleeve, $\epsilon = 4$.

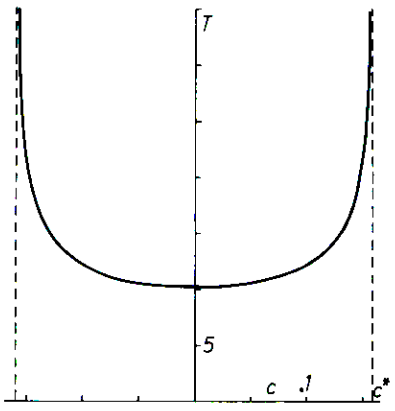

Fig. 11 bis. Periods of the blue sleeve, $\epsilon = 4$.

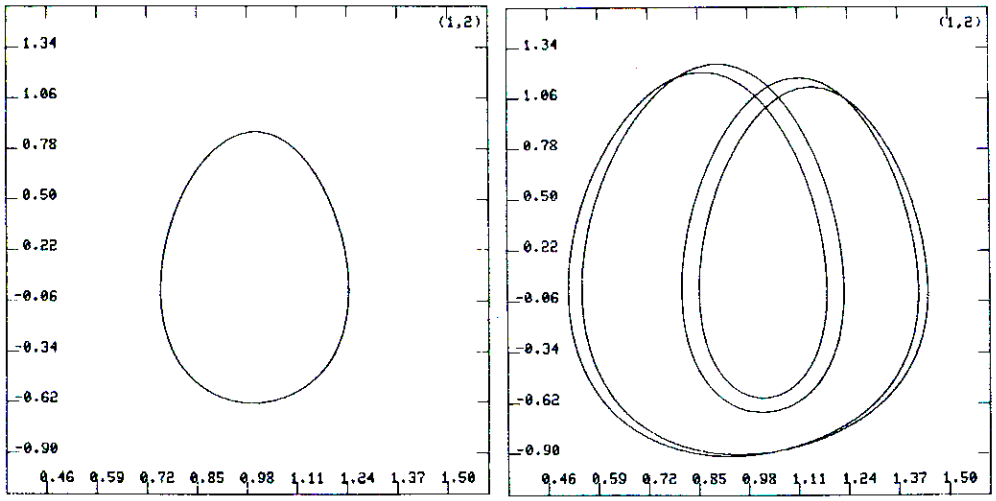

(a) b = 2.000 (c) b = 2.840

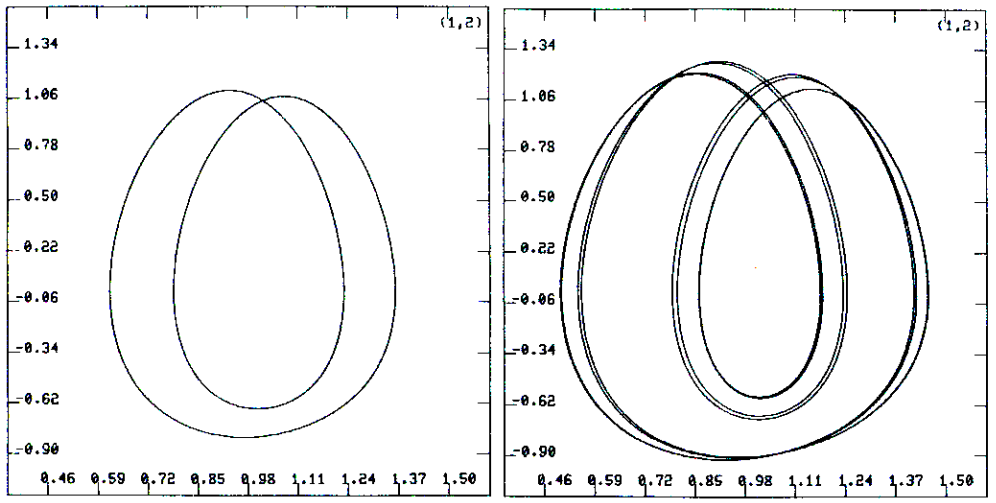

(b) b = 2.500 (d) b = 2.870

Fig. 12. Period doubling bifurcation sequence in the Van der Pol system with standard bias and forcing, with ϵ =4, a = 1, ω = 3, and amplitude, b.

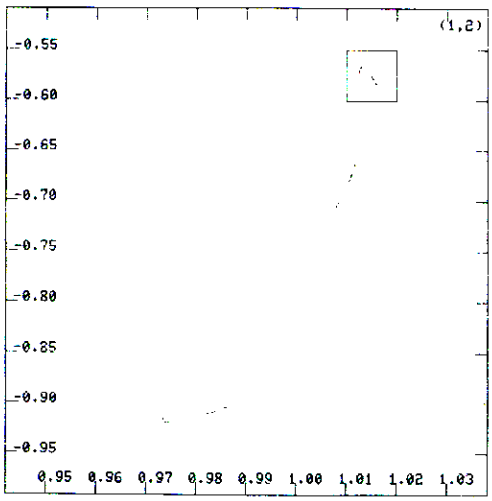

(a) full Poincare section

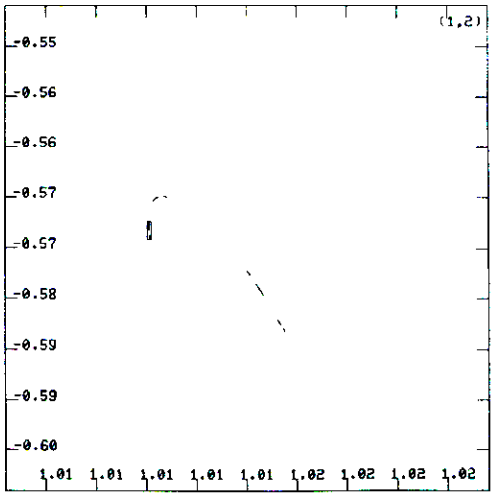

(b) enlargement of the box

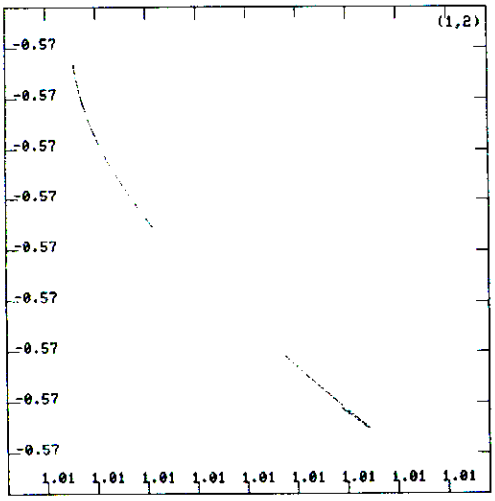

(c) further enlargement

Fig. 13. Sections of the chaotic attractor (32-SA) in the forced Van der Pol system, as in Fig. 12, except b = 2.880.

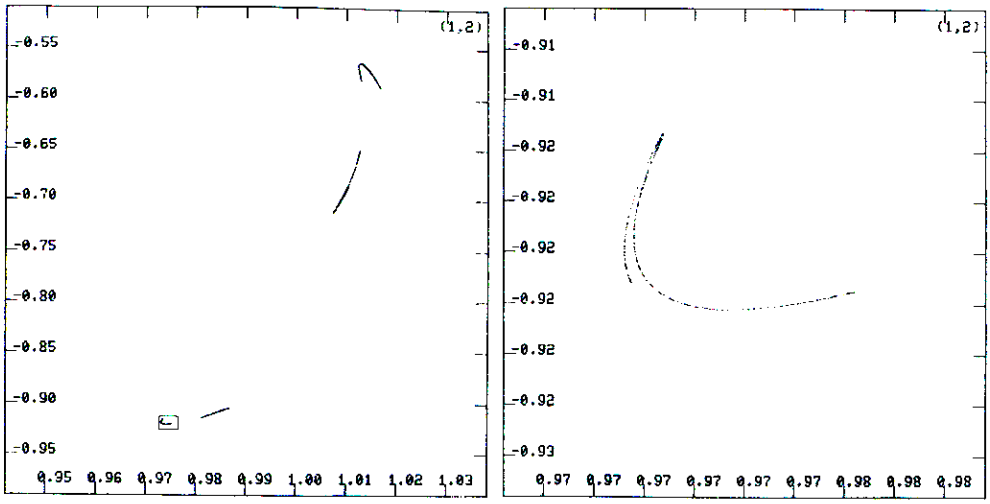

(a) full Poincare system (b) enlargement of the box

Fig. 14. Sections of the chaotic attractor (4-SA) in the forced Van der Pol system, as in Fig. 12, except b = 2.885.

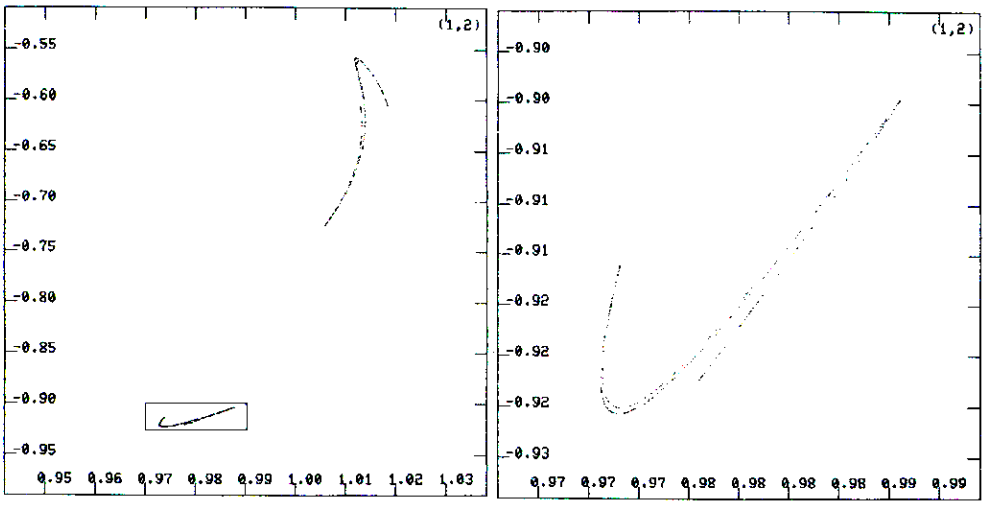

(a) full Poincare system (b) enlargement of the box

Fig. 15. Sections of the chaotic attractor (2-SA) in the forced Van der Pol system, as in Fig. 12, except b = 2.890.

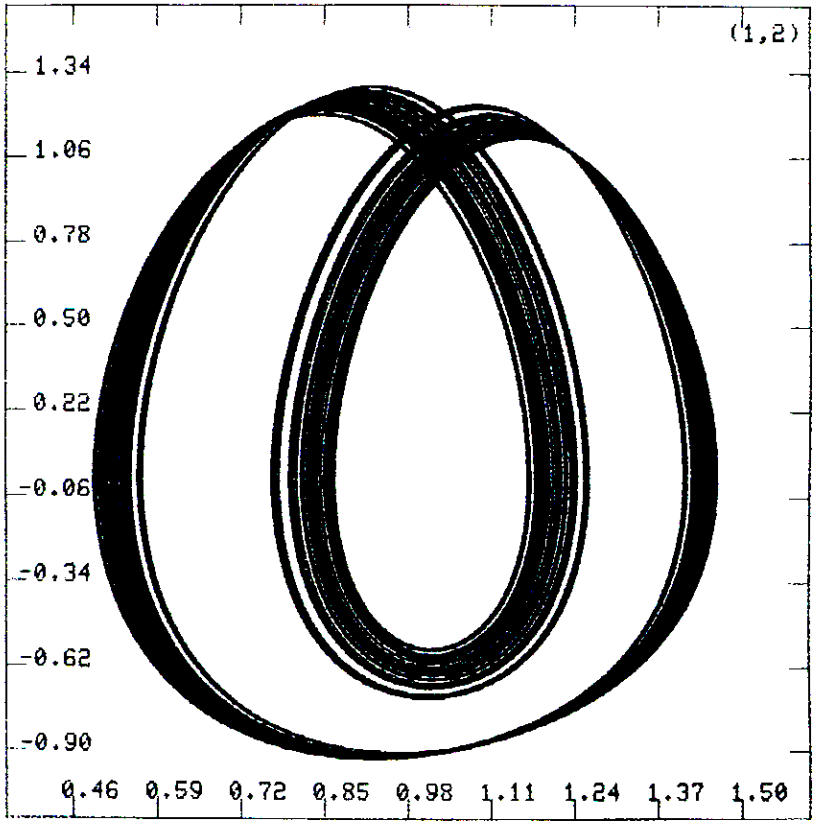

Fig. 16. Chaotic attractor in the forced Van der Pol system, as in Fig. 15.

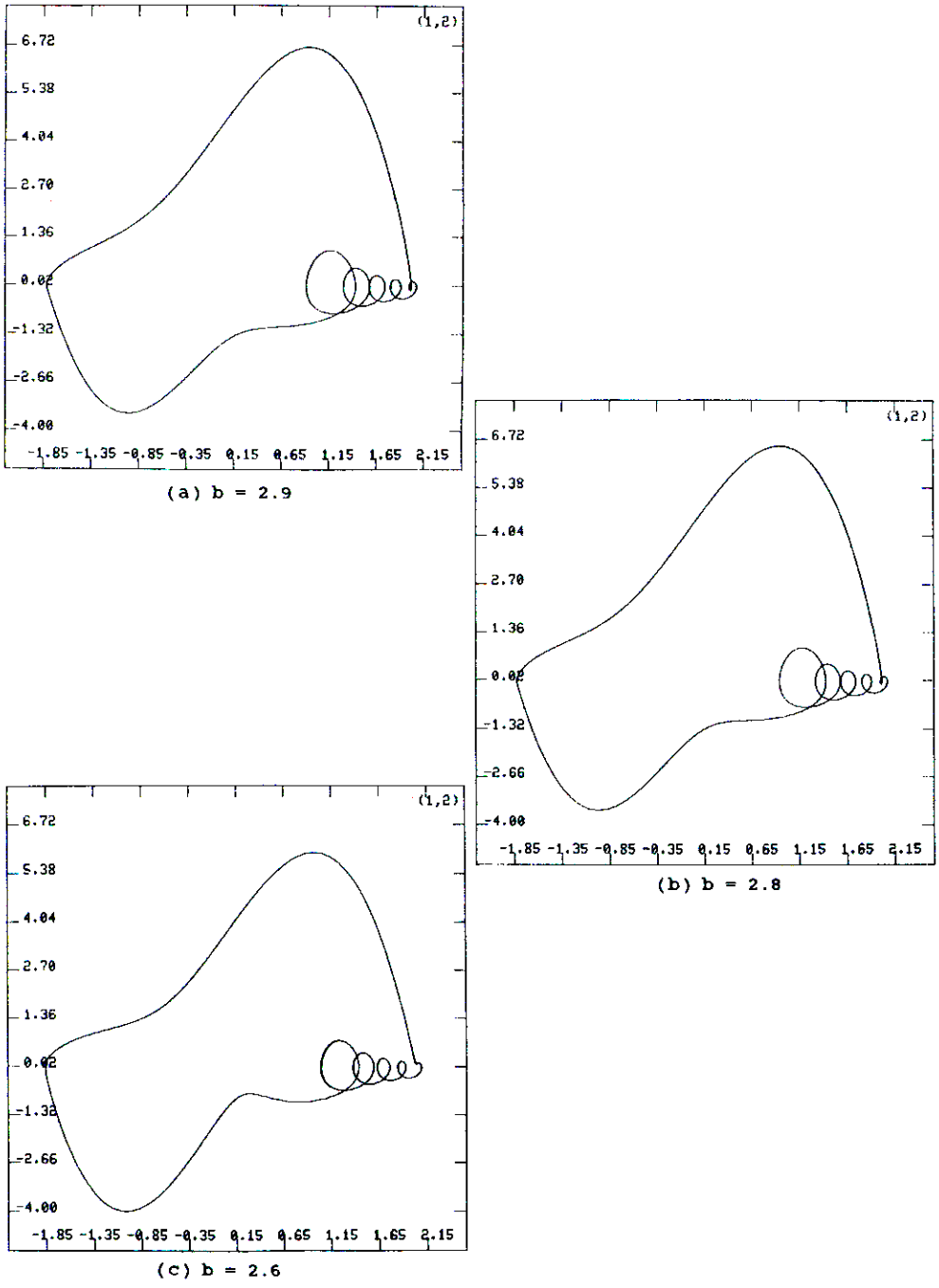

Fig. 17. Alternative periodic attractor (7-PO) in the forced Van der pol system, as in Fig. 12.

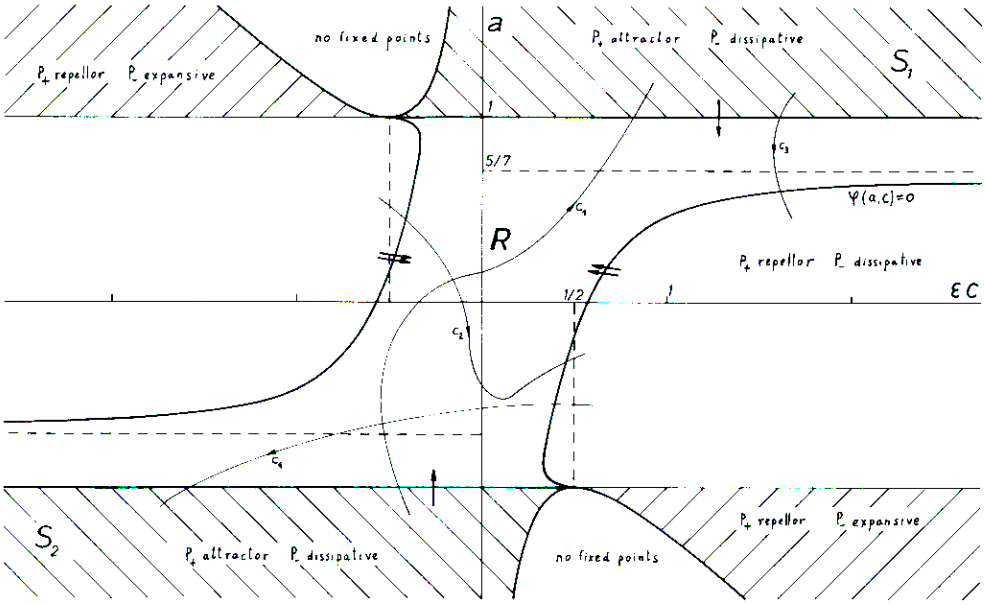

Fig. 18. Bifurcation set of the double biased Van der Pol system, with $\epsilon = 1$.

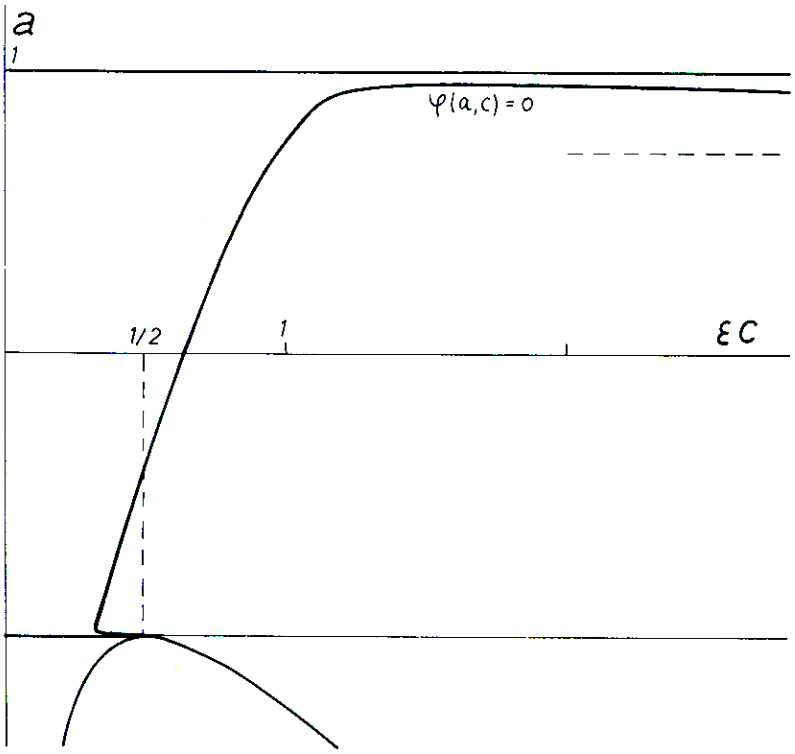

Fig. 18 bis. Bifurcation set of the double biased Van der Pol system, with $\epsilon = 4$.

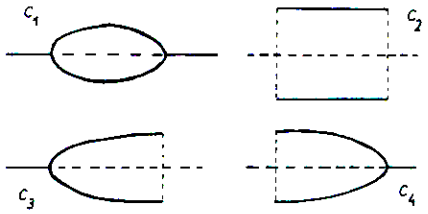

Fig. 19. Bifurcation diagrams for four selected arcs in the control plane, Fig. 18.

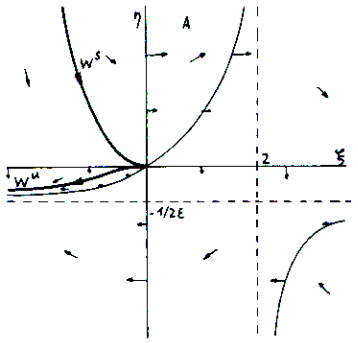

Fig. 20. Vectorfield corresponding to the bifurcation point of codimension two in Figs. 18, 18bis, and 19, showing the stable and unstable manifolds of the doubly degenerate critical point.

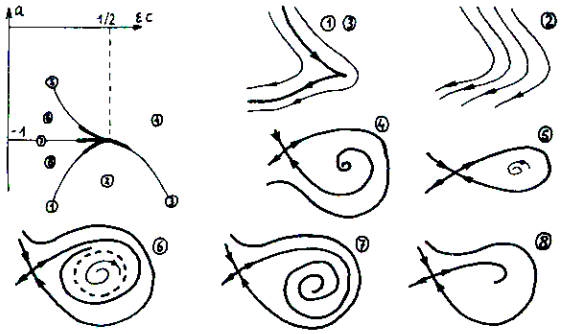

Fig. 21. Bifurcation tableau for the bifurcation of codimension two.

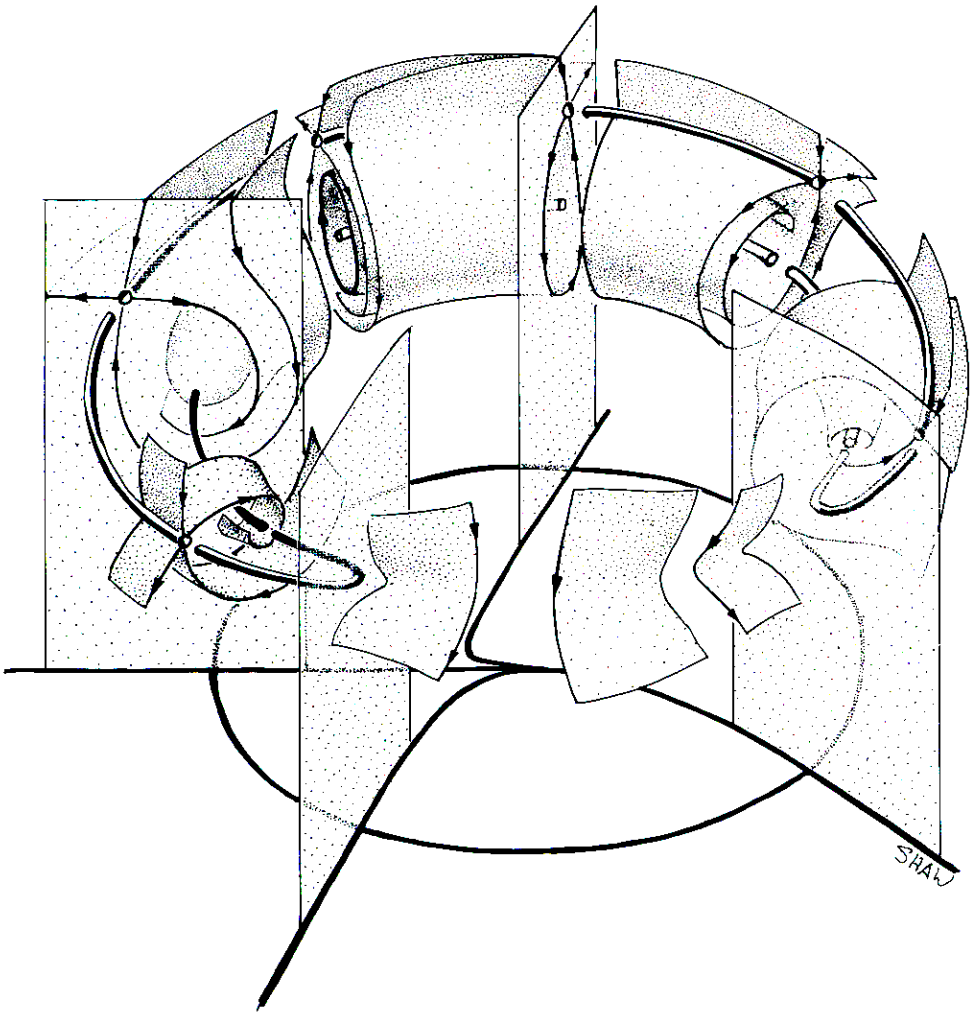

Fig. 22. Response diagram for a cycle around the bifurcation point of codimension two: the blue goblet.

(a) The goblet within the separatrix.

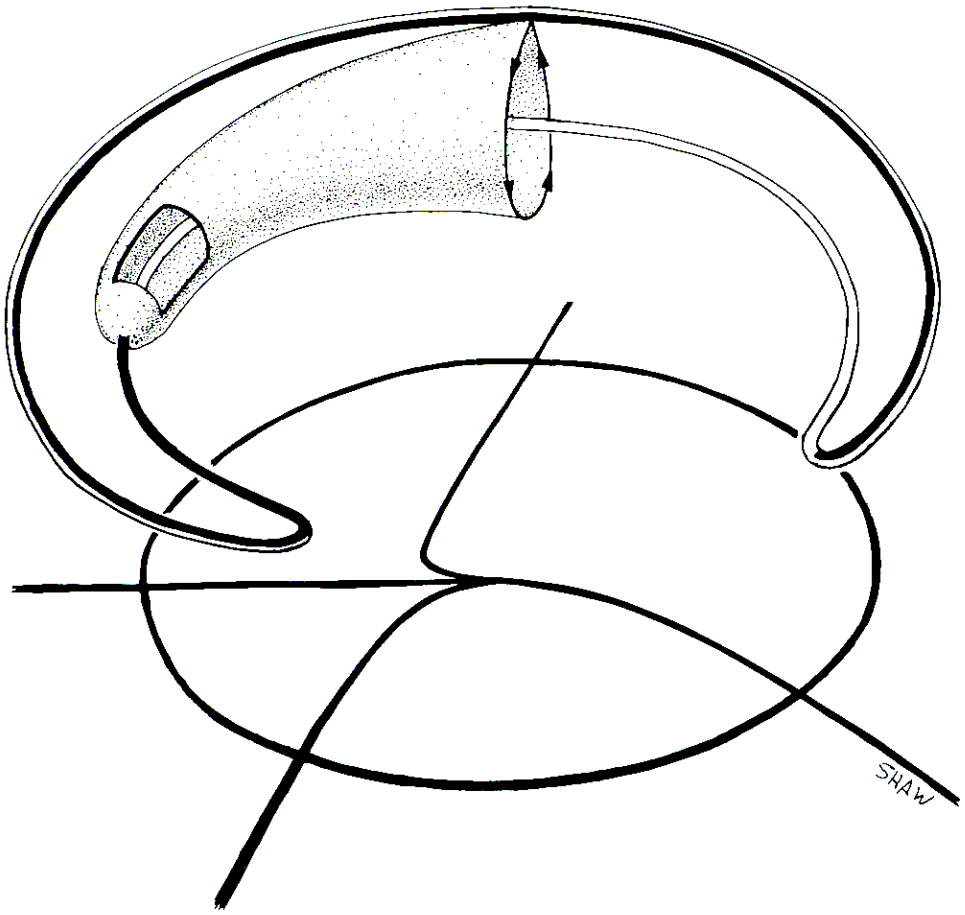

(b) Same, with the separatrix removed for a better view.

Ralph ABRAHAM
University of California
Department of Mathematics
Santa Cruz, CA 95064
U. S. A.

&

Carles SIMO
Universitat de Barcelona
Facultat de Matematiques
Gran Via 585, Barcelona 7
SPAIN